J Mater Sci (2008) 43:5772–5783
DOI 10.1007/s10853-008-2889-2

The interaction of magnesium in hydration of C_3S and CSH formation using ^{29}Si MAS-NMR

L. Fernandez · C. Alonso · C. Andrade · A. Hidalgo

Received: 11 March 2008 / Accepted: 18 July 2008 / Published online: 9 August 2008

Abstract Hydration of tricalcium silicate in hydrothermal conditions in the presence of magnesium oxide has shown changes in the formation of CSH gel structure (Calcium silicate hydrates). The new CSH incorporates magnesium ions, brucite, but a weak presence of portlandite. The magnesium oxide would hinder the precipitation of portlandite. The characterization of CSH gel by ^{29}Si MAS-NMR with various CaO/SiO_2 ratios would point out that: (1) A dreierketten structure of the CSH for low $CaO/SiO_2 < 1$, with some defects (Q^3 defect and Q^{2v}) in its structure is confirmed. Some magnesium ions are incorporated in the octahedral sites, in the interlayer space of the dreierketten pattern. (2) For the CSH gels with CaO/SiO_2 ratios > 1, magnesium ions would be incorporated in the silicate chains of the CSH gel in a tetrahedral coordination. Although, the low MgO/CaO ratios of CSH gels indicate that the magnesium incorporation in CSH chain is low.

Introduction

Calcium silicate hydrates (CSH) are natural minerals that appear in a variety of geological settings, but also are the main components resulting from cement hydration. Amorphous CSH gel is formed during hydration of tricalcium silicate (C_3S) [1] which follows a slow kinetic process at room temperature, (after 28 days only approximately 70% of C_3S has reacted with water); meanwhile, in hydrothermal conditions at 100 °C and after 14 days, the C_3S is almost completely transformed into CSH gel [2].

The CSH gel has a poor crystalline structure of variable composition [1], which is controlled by the CaO/SiO_2 (Ca/Si) ratio and $[Ca^{2+}]$ [3]. Its stoichiometry ranges from $0.66 < Ca/Si < 1.7$ [3–8]. A large amount of Portlandite ($Ca(OH)_2$) precipitates simultaneously with CSH formation for $CaO/SiO_2 > 1.5$.

The more accepted structure for CSH gel from cement hydration was proposed by Taylor [1] who considered two forms, CSH (I) and CSH (II), similar to tobermorite and jennite, respectively; although other structural models for CSH has been proposed more recently [9, 10]. A model structure of CSH gel is considered in Fig. 1, which presents some analogy with tobermorite.

For $Ca/Si = 0.66$, linear chains of silicate tetrahedral sheets of SiO_2 associated to an octahedral sheet of CaO with a Te–Oc–Te structure, but with some defects [11–13] are formed. The SiO_2 chains are constituted of dimers, ($Si(Q^2)$), connected by bridging tetrahedron ($Si(Q^{2p})$), (dreierketten pattern). Silicate tetrahedron ($Si(Q^{2p})$) are balanced by ions of H^+ in the interlayer space. As the Ca/Si ratio increases above 0.8, the H^+ ions are substituted by Ca^{+2} ions into the interlayer space.

For Ca/Si ratio from 1.5 to 1.7 and $(Ca^{2+}) \geq 22$ mM/L, $Ca(OH)_2$ (Portlandite) precipitates in equilibrium with the CSH gel, a shortening of the silicate chains takes place as Ca content increases [14, 15], and the structure of this CSH is mainly constituted by silicate dimers.

L. Fernandez · C. Alonso (✉) · C. Andrade · A. Hidalgo
Institute of Construction Science "Eduardo Torroja"(C.S.I.C.), Serrano Galvache 4, 28033 Madrid, Spain
e-mail: mcalonso@ietcc.csic.es

L. Fernandez (✉)
Institut de Ciència dels Materials de la Universitat de Valencia (ICMUV), Universitat de Valencia, P.O. Box 22085, 46071 Valencia, Spain
e-mail: lorenzo.fernandez@uv.es

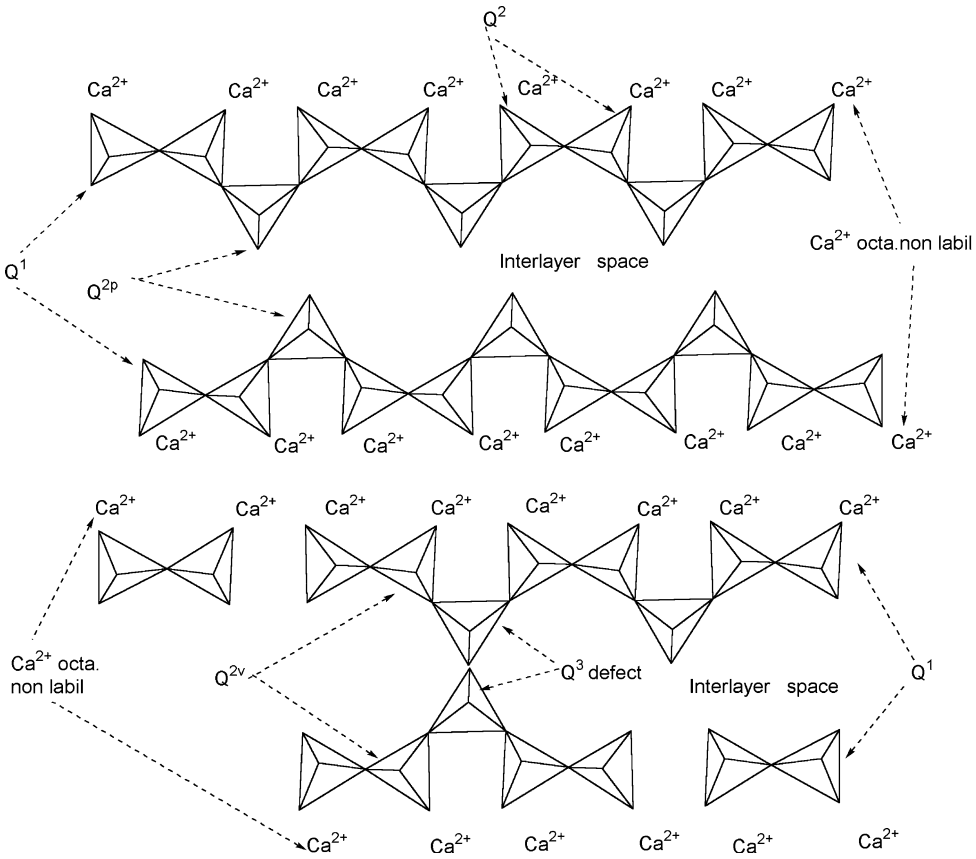

Fig. 1 The structure of the CSH gel for CaO/SiO_2 ratios < 1 [12]

The presence of other compounds, such as Mg, during the hydration of C_3S can induce modification in the hydrated product, for instance the incorporation of Mg^{2+} into the structure [16–19]. Pytel [17] and Fernandez et al. [16] identified the possible incorporation of magnesium into the CSH structure and observed a new phase attributed to the formation of a magnesium silicate hydrate (MSH), but its structure is still unknown. Fernandez et al. [16] found that the CSH was constituted by two main phases, with different content in Mg, using SEM and EDAX analysis, areas of CSH rich in magnesium, attributed to MSH, with other mainly composed by CSH gel but with less magnesium content. MSH gel formation is only considered into the CSH gel of low CaO/SiO_2, while in the CSH of high CaO/SiO_2 a four-fold coordination of Mg inserted in the silica chains of the C–S–H gel has been proposed.

The aim of present paper is to corroborate the incorporation of magnesium into the CSH gel structure as C_3S is hydrated in presence of MgO. High-resolution solid-state NMR of ^{29}Si MAS-NMR, X-ray diffraction, and thermogravimetric analyses were performed to verify the chemical substitution and the modification introduced by the presence of Mg in the equilibriums of the pore solution and hydrated phases.

Experimental section

Samples preparation

Solid samples of different CaO/SiO_2 ratio were hydrated in the presence of magnesium oxide. The synthesis was carried out by mixing synthesized C_3S with silica gel to obtain various CaO/SiO_2 ratios, as indicated in Table 1.

Lafarge Society prepared the synthesized C_3S. Its chemical composition was 24.92% (SiO_2) and 62.49% (CaO), which gives a CaO/SiO_2 molar ratio 2.7.

Silica gel of 99.5% of purity was previously dehydrated at 100 °C for 8 h. Magnesium oxide was also added to the mixture in a MgO/CaO molar ratio = 0.49. Magnesium oxide was obtained from magnesium hydroxycarbonate (99.5% purity) previously decarbonated and dehydroxylated at 1000 °C for 14 h. The homogeneity of the reactants was guaranteed by stirring in acetone.

Hydration process and composition of components

The hydration reaction was performed in hydrothermal conditions at 100 °C (autoclave) for 23 days in the presence of decarbonated water at a water/solid ratio of 5.

Table 1 Mass of each chemical component mixed for the synthesis of the samples. The CaO/SiO_2 ratio of C_3S is 2.7

Samples	C_3S (g)		Silica gel (g)	MgO (g)	$(CaO)/(SiO_2)$	$(MgO)/(CaO)$
	CaO (62.49 wt%)	SiO_2 (24.92 wt%)				
S1	1.5		1.575	0.332	0.53	0.49
S2	1.5		1.0412	0.332	0.72	0.49
S3	1.5		0.604	0.332	1.04	0.49
S4	1.5		0.302	0.332	1.52	0.49

After hydration, solid and liquid phases were separated by filtration. The moist solid samples were dried with acetone to stop further hydration. Chemical analysis of Mg, Si, and Ca were performed in the residual liquids and the precipitated solids. Microstructural characterization of the solids was also performed. Before the chemical analyses, the samples were dissolved by an acid treatment. Chemical compositions were obtained by Atomic Absorption Spectrometry (AAS, Perkin–Elmer 1100B).

Techniques for characterization of solid phase

X-ray diffraction (XRD) technique was used to identify the crystalline phases, which were formed during the hydrothermal synthesis. XRD data of the C_3S and hydrated solids were recorded using a Phillips PW1820, powder diffractometer with Cu$K\alpha$ radiation. The goniometer speed was 0.020°/s. Software from Phillips was used to characterize the mineralogical crystalline phases.

For the thermogravimetric (TG) and differential thermogravimetric analyses (DTA) of hydrated solids, a Netzsch simultaneous analyser, model STA 409 was used with a heating ratio of 4 K min^{-1} under a nitrogen flow of 100 cm^3 min^{-1}. The analyzed mass per sample was about 50 mg.

^{29}Si MAS-NMR spectra were recorded at the ^{29}Si resonance of 59.572 MHz using a Varian VXR 300S spectrometer, with a spinning speed of 4 kHz in a double bearing 7 mm ZrO_2 rotor. Spectra were accumulated using Bloch decay pulse sequences of Π/2 and high power ^1H decoupling with a 60 kHz radio frequency field. A recycle time of 59 s was used. The number of scans was 1,000. Tetramethylsilane (TMS, $Si(CH_3)_4$) was used as a reference. The spectra were simulated using a modified version of the Winfit program [20].

Results

Chemical analysis of the solid and of the liquid phases

In Table 2, the composition of the liquid phase obtained after the hydrothermal hydration is included for S1–S4 samples. Calcium and silicon ions are present in the liquids, and an increasing content of calcium ions in solution is detected as the CaO/SiO_2 ratio of the solid increases, whereas with silicon ion a decrease is measured. Magnesium ions are detected into the liquids but at trace levels. The pH of the liquid phase increases as it does with the CaO/SiO_2 ratio.

Thermogravimetric analysis of the samples

Thermogravimetric analysis is used to quantify the bound H_2O, brucite, $Ca(OH)_2$, and carbonates, (TG and DTA curves, Fig. 2a and b). The quantitative weight losses from TG are given in Table 3. The second derivatives of thermogravimetric analyses (DTG) are presented in Fig. 2a, to better identify the endothermic peaks related to chemical transformations of hydrated solids taking place in hydrothermal hydration.

Table 2 Chemical analyses of the liquid and the solid phases

Samples	Liquid phase				Solid phase					
	pH	Ca^{2+} (ppm)	Si^{4+} (ppm)	Mg^{2+} (ppm)	CaO (wt%)	SiO_2 (wt%)	MgO (wt%)	L.O.I (wt%)	$(CaO)/(SiO_2)$	$(MgO)/(CaO)$
S1	9.76	81.9	7.28	0.2	28.41	45.80	8.33	20.60	0.66	0.41
S2	11.98	164.3	1.74	0.2	29.31	35.21	8.72	22.47	0.88	0.42
S3	12.58	540.1	0.37	0.2	37.61	31.56	10.92	27.88	1.26	0.40
S4	12.72	692.6	0.63	0.2	43.83	25.64	12.70	23.57	1.81	0.41

The uncertainty on the weight percentages of the solids and the concentration of the liquids are given with a precision of ±10%

L.O.I: Loss of Ignition

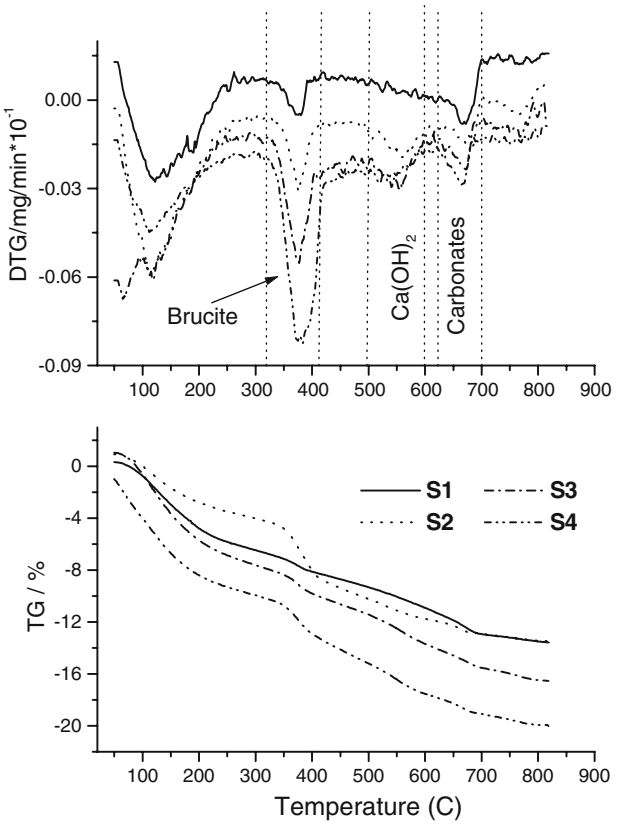

Fig. 2 Thermogravimetric analysis of the samples S1–S4

Most of the free water, still present in the samples, is removed until 100 °C. In the range of 100–300 °C, a large endothermic peak is observed due to the loss of water from CSH. The amount of binding water is less for S4, probably due to a lesser CSH formation or due to a CSH structure containing less water molecules. The decomposition of the brucite gives the characteristic endothermic peak at about 320–400 °C that increases in size as CaO/SiO_2 ratio of the mixture also does. The endothermic peak of the calcium hydroxide is not well identified, even in the S4 sample with $CaO/SiO_2 = 1.81$. These results suggest that the presence of magnesium oxide during hydration of C_3S hinders the precipitation of $Ca(OH)_2$. Finally, a small endothermic peak between 620 °C and 700 °C is formed due to the decomposition of the carbonates. The presence of the carbonates has been attributed to the reaction of the samples with the CO_2 of the air into the autoclave atmosphere or during sample preparation for characterization tests forming calcium and magnesium carbonates.

X-ray diffraction results

XRD diffractogram of the anhydrous synthesized C_3S is given in Fig. 3. Low intensity reflections attributed to C_2S impurities are detected, but the main reflections are due to C_3S.

The good resolution of the XRD diffractogram of sample S4 allows to identify the presence of traces of unhydrated material as, C_3S and probably C_2S. The same is detected in samples (S2 and S3), but the reflections overlap with crystalline phases of CSH. Only sample S1 does not show any anhydrous phases after 23 days in hydrothermal hydration.

All hydrated samples show the presence of calcium carbonates as calcite, aragonite, or vaterite. The presence of magnesite is detected in S1, S2, and S3, but the peaks overlaps with those of $CaCO_3$; the presence of $Ca_{1.5}SiO_{3.5} \cdot xH_2O$ is only detected in S1. Tobermorite, plombierite, and $CaO \cdot SiO_2 \cdot H_2O$ are also identified in the sample S1. Portlandite is probable in samples S3 and S4 but the reflections are low. The formation of crystallized brucite is detected in S2, S3, and S4. The most intense reflection of brucite, at 37.983°, increases from S2 to S4 as it does in the thermogravimetric analysis. No crystalline magnesium silicates have been identified by XRD.

^{29}Si MAS-NMR results

For the interpretation of ^{29}Si MAS-NMR spectra, the silicate tetrahedra are designated as Q^n, where Q represents the silicon tetrahedron bonded to four oxygen atoms and n the connectivity, i.e., the number of other Q units attached to one specific SiO_4 tetrahedron. Thus, Q^0 denotes the monomeric orthosilicate anion SiO_4^{4-} (nesosilicate), Q^1 represents an end group of a chain, Q^2 a middle group, Q^3 a chain branching site, and Q^4 a three-dimensionally fully cross-linked group. The isotropic chemical shift (δ^{iso}) of the ^{29}Si nuclei allows to obtain information concerning the organization of the tetrahedral links [21, 22].

Table 3 Weight losses at different temperature ranges

Samples	Weight loss (%)			
	Temperature range (°C)			
	100–250 bound H_2O	320–400 $Mg(OH)_2$	500–600 $Ca(OH)_2$	620–700 carbonates
S1	5.1	1.4	None	1.6
S2	6.3	2.2	None	1.4
S3	5.3	3.2	Traces	1.3
S4	3.5	4.6	Traces	1.0

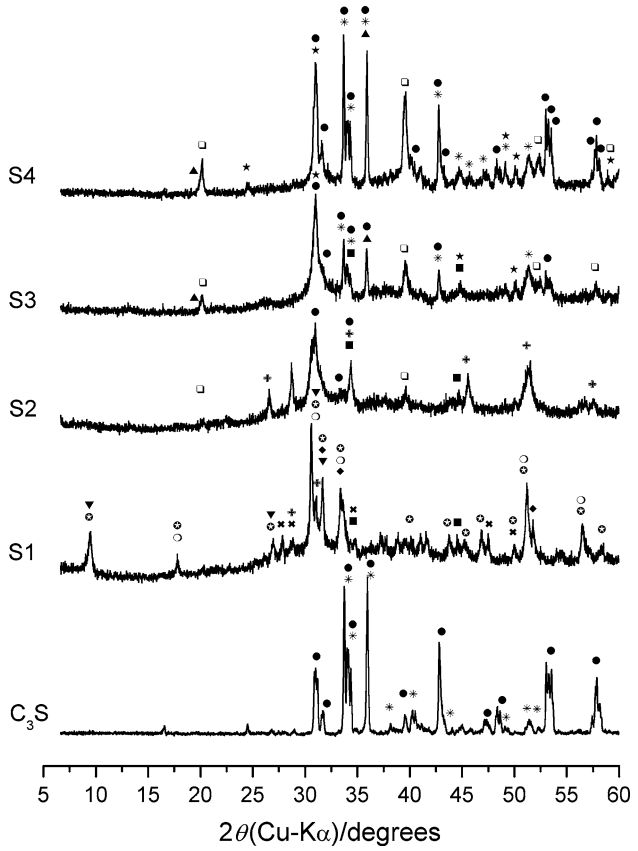

Fig. 3 X-ray diffractograms of C_3S and the samples S1–S4. Key to phases: C_3S, ●; C_2S, ✳; Tobermorite 11Å, ▼; $CaO \cdot SiO_2 \cdot H_2O$, ✪; Plombierite, ❍; $Ca_{1.5}SiO_{3.5} \cdot xH_2O$, ◆; Brucite, ❒; Portlandite, ▲; Magnesite, ■; Calcite, ★; Vaterite, ✚; Aragonite, ♂

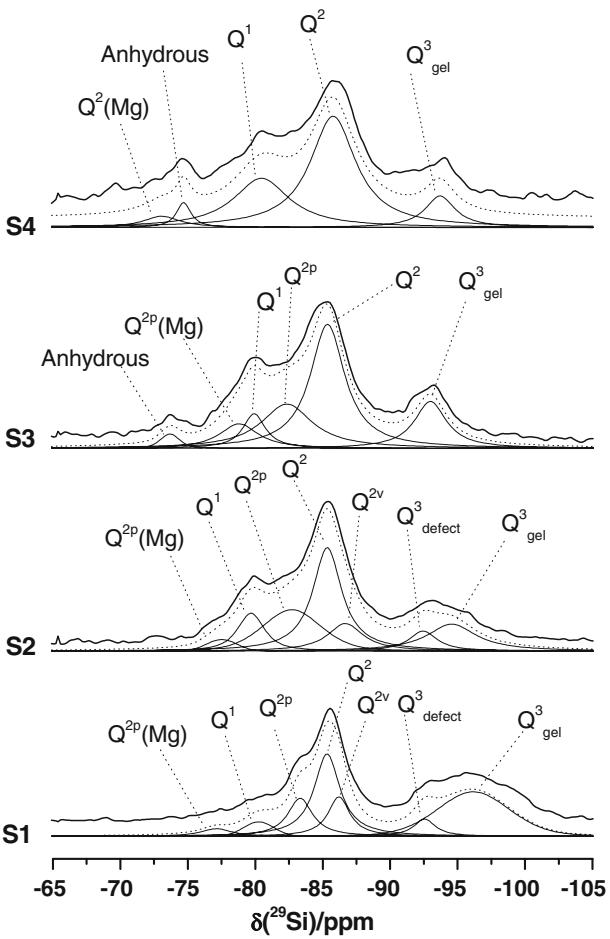

Fig. 4 ^{29}Si MAS-NMR spectrum of the samples S1–S4. The isotropic chemical shifts are referenced to the T.M.S ($Si(CH_3)_4$). The thick solid line represents the experimental spectrum. The other solid lines are the Gaussian components of the silicate tetrahedra Q^n and the deconvolutions

The deconvolution model of the different phases in the spectra has been carried out considering Gaussian lines: Q^1 and Q^2 tetrahedra to simulate CSH phases, Q^0 attributed to the non-hydrated phases C_3S and C_2S, and Q^3 and Q^4 associated with silica gel [11, 14, 15, 23–31]. However, the deconvolution of the spectra by using solely Q^0, Q^1, Q^2, Q^3, and Q^4 groups, led to a deficient fitting of all NMR signals. In the present model, the results of dipolar correlation model of CSH have been used [12, 13, 32] for the deconvolution and better interpretation of the NMR spectra. This model establishes for CSH gel with CaO/SiO_2 ratio < 1 the following assignments: (1) $Si(Q^1)$ at -78.9 ppm, (2) $Si(Q^{2p})$ at -82.1 ppm, (3) $Si(Q^2)$ at -85.3 ppm, (4) $Si(Q^{2v})$ (-87.3 ppm), and (5) $Si(Q^3$defect) (-91.5 ppm). Afterwards, for each CaO/SiO_2 ratio used the details of the model are developed. In all samples, the NMR signal shows excess of silica gel.

The spectra of the different samples are given in Fig. 4 and the quantitative values of the different assignments from the deconvolutions are presented in Table 4.

NMR identification of samples with CaO/SiO_2 ratio ≤ 1 (S1 and S2)

The deconvolution of the NMR spectra of samples S1 and S2 with CaO/SiO_2 ratios < 1, has been performed taking into account the following assumptions [12]:

(1) The structure of CSH gel is similar to that of the tobermorite.
(2) A Dreierketten structure of CSH gel is accepted, what implies that the intensity of the resonance of the bridging tetrahedra (Q^{2p}) is about half of the intensity of Q^2 resonance (non-bridging tetrahedra), i.e., $Q^2/Q^{2p} = 2$.
(3) The appearance of Q^3 defects, due to the connection between two bridging tetrahedra (Q^{2p}), which modifies the Si–O–Si angle between the non-bridging tetrahedral, denoted as Q^{2v} tetrahedral, as referred by [12, 13]. The intensity of the resonance of Q^3 defect is

Table 4 Deconvolution results of the ^{29}Si MAS-NMR spectra for the samples S1–S4

Samples	$\delta(^{29}Si)$ and integration (%)									
	New resonance		Anhydrous	CSH					Silica gel	
	Q^2(Mg)	Q^{2p}(Mg)	Q^0	Q^1	Q^{2p}	Q^2	Q^{2v}	$Q^3{}_{defect}$	Q^3	Q^4
S1	–	−77.1 (5)	–	−80.3	−83.3 (15)	−85.3 (30)	−86.2 (10)	−92.6 (5)	−96.2 (35)	–
S2	–	−77.5 (5)	–	−79.7 (10)	−82.7 (15)	−85.3 (30)	−86.7 (10)	−92.4 (5)	−94.6 (25)	–
S3	–	−78.8 (10)	−73.7	−79.9 (10)	−82.3 (20)	−85.4 (40)	–	–	−93.0 (20)	–
S4	−73.1 (5)	–	−74.7 (5)	−80.5 (30)	–	−85.8 (50)	–	–	−93.7 (10)	–

The isotropic chemical shifts are in ppm and the integrations are given inside of the parenthesis

about half of the Q^{2v} resonance [12], i.e., $Q^{2v}/Q^3_{defect} = 2$.

The deconvolutions of the NMR spectra by using the suggestions of bibliography on the structure of CSH related to Q^1 and Q^2 did not allow to obtain a satisfactory result. Additional information is observed in RMN spectra that could confirm the presence of magnesium sites in CSH gel [16]. The number of studies published on this topic show that the choice of a CSH model is not obvious, indeed the debate on the structure of CSH gel is open and several publications appear, as the review from Nonat [9, 10]. There exist several models that try to describe the disordered structure of CSH gel using the Defect Tobermorite Model [11–13]. This model is based on the conclusions of previous papers using NMR technique for solids, such as NMR Cross-Polarization (CP) measurements [33], Double Quantum Si–Si correlation [32], 2D H–Si HECTOR experiments [32], and Molecular Dynamics calculations [34, 35].

The Klur model [11–13] supports a structure for CSH gel similar to that of tobermorite, with significant concentrations of different types of defects. The CSH spectra of present work fit well using the Defect Tobermorite Model. Although, the first adjustment to the model showed that the spectra were not fully fitted; however, the addition of new resonances improved the final fitting. These new resonances will be used to discuss the addition of new Gaussian lines.

The Q^1 resonance is observed for S1 (less than 5%) and S2, given in Table 4. Q^2 and Q^{2p} signals appear in S1 and S2 samples. The Q^2/Q^{2p} ratio of the intensities confirms the dreierketten pattern of CSH for S1 and S2, with one bridging tetrahedra for every two non-bridging ones. Also, the Q^3 defect with the associated resonance corresponding to Q^{2v} tetrahedra appears from the deconvolution of NMR spectra for S1 and S2.

NMR of samples with CaO/SiO$_2$ ratio ≥ 1 (S3 and S4)

The typical Q^1 and Q^2 resonances from CSH are also observed. The intensity of the Q^1 resonance increases for higher CaO/SiO$_2$ ratios, indicating the rupture of silicate chains.

Q^2 and Q^{2p} signals appear clearly in S3. The Q^2/Q^{2p} ratio of the intensities confirms the dreierketten pattern of CSH also for S3 sample, with one bridging tetrahedra for every two non-bridging ones. From the deconvolution of S3, the Q^3 defect and the associated resonance corresponding to Q^{2v} tetrahedra do not appear.

Sharp peaks typical of the monomeric orthosilicate anion (nesosilicate) and characteristic of a crystalline phase, denoted as Q^0, and attributed to anhydrous (C_3S) are observed in the samples S3 and S4. Infact, in the region of Q^0, the bottom of the signal is different for S4 in comparison with the same region in the spectrum of S3 (see Fig. 4). The sample S3 displays just the sharp resonance of unreacted C_3S, but it is clear for S4 that a new resonance appears at downfield shift from the resonance of C_3S. This new resonance appears at −73.1 ppm. Some authors for the fitting of C_3S NMR spectrum used 12 [36] and 8 [37] Gaussian and/or Lorentzian peaks. The number of Gaussian and/or Lorentzian peaks should depend on the number of the non-equivalent Si sites in the crystalline C_3S phase. As there exists various crystal structures for C_3S [1], an accurate identification of the crystalline structure should be previously performed. There are some publications on Rietveld refinements applied to different crystalline phase of tricalcium silicate (C_3S) [38–42] in which the number of the non-equivalent Si sites is high. As the intensity and the resolution of the anhydrous part of the ^{29}Si MAS-NMR spectra (S3 and S4 in Fig. 4) are relatively low, therefore, an adjustment by various Gaussian peaks should imply to fix some parameters such as the isotopic chemical shift and the line-widths. Hence, it would seem non adequate for the purpose of this paper to perform an adjustment through this way which could give a truncate information. Thus, the anhydrous part has been fitted by only one Gaussian peak and it is attributed to C_3S.

In summary, the NMR results show that new resonances in samples S1 to S4, appear at −77.1 ppm (S1), −77.5 ppm (S2), −78.8 ppm (S3), and −73.1 ppm (S4).

These resonances were not previously described for CSH structure in the literature [11, 13, 14, 23–26, 43].

Discussion

The chemical analyses of the liquid phases after hydration show similarities with the results of Cong [11] without the presence of magnesium and it also shows some differences:

- pH of the liquids increases with the increasing CaO/SiO_2 ratio [11], but in the presence of Mg, they lead to higher pHs, as it is shown in Fig. 5 (left).
- The evolution of Ca^{2+} vs. CaO/SiO_2 ratio also represented in Fig. 5 (right) describes the same tendency with and without Mg^{2+} [11]. The main difference is the change in the slope of the curve of the present work, which occurs for $[Ca^{2+}] = 12$ mM/L, instead of 17 mM/L found by [11]. The slope change is associated with the precipitation of portlandite [11]. In the present study, the precipitation of portlandite is not well identified neither by TG nor by XRD. The formation of brucite during C_3S hydration in hydrothermal conditions in the presence of Mg is favored. For all the samples, the MgO/CaO ratio of the solids is constant and there are approximately two calcium ions per each magnesium ion.

By using SEM-EDAX, Fernandez et al. [16] showed the presence of magnesium into the C–S–H gels. The chemical balance of magnesium has been done to confirm that:

(1) The total magnesium content is given in Table 2.
(2) For each sample, the amount of magnesium in the form of brucite can be calculated using thermogravimetric analysis (Table 3).
(3) Thermogravimetric analysis also shows the presence of some carbonates. In this case, it is assumed that all are fully constituted by magnesite although the XRD shows the presence of $CaCO_3$. From these calculations, some magnesium appears to be incorporated into the C–S–H gel. The MgO/CaO ratios of C–S–H gels demonstrate that the magnesium incorporation is weak.

Structure of C–S–H in the presence of MgO for CaO/SiO_2 ratios < 1

Brucite has been quantified by TG in S1 sample, however, in the XRD diffractogram, this structure does not appear, probably due to a poor crystallization.

The ^{29}Si MAS-NMR results of the samples (S1–S2) are in agreement with the dreierketten pattern of C–S–H proposed in the bibliography [1, 12–14, 24].

For the sample S1, the dreierketten pattern is maintained (Table 4); moreover, the NMR signal of C_3S is not observed in accordance with XRD results. As C–S–H gel is in contact with a concentrated electrolytic solution of Mg^{2+} ions, the chemical shifts are modified. Also, it is observed as a large peak corresponding to tetrahedra defects (Q^3 defect), which are associated with the Q^{2v} tetrahedra.

The S2 sample denotes a peak at −79.7 ppm, which corresponds to Q^1 tetrahedra, i.e., silicon tetrahedra at the end group of a chain, and an extra peak Q^{2p}(Mg), at −77.5 ppm (Table 4). For S1 sample, an extra peak Q^{2p}(Mg), at −79.1 ppm is also observed, which is slightly shifted of the extra peak Q^{2p}(Mg) of S2 sample. Also, as in sample S1, the NMR signal of the Q^3 tetrahedron shows a higher intensity.

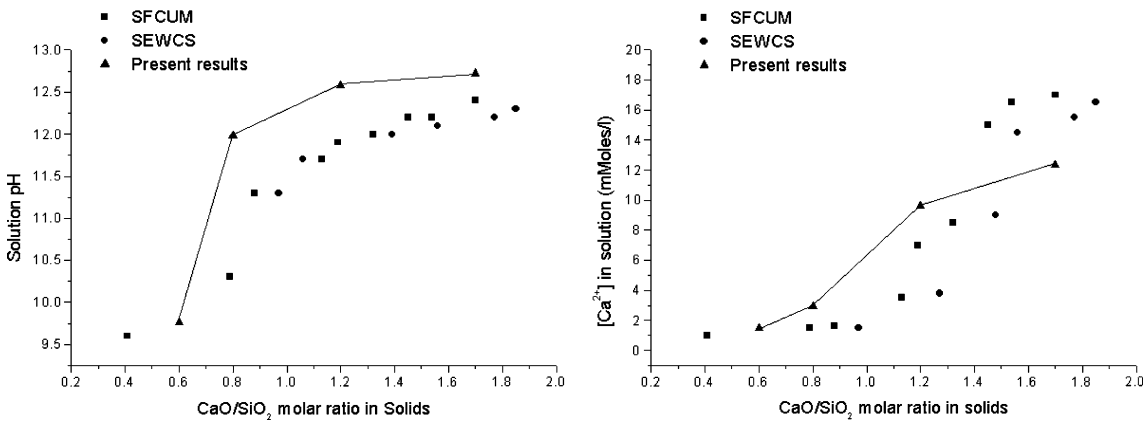

Fig. 5 Observed relationships between solution pH and C/S (CaO/SiO_2) of the solid CSH (left) and solution Ca^{2+} concentration and C/S ratio of the solid CSH (right) for SEWCS and SCFUM series [11] and present results. SEWCS and SCFUM are the CSH synthesized from two different methods

For both the samples, following considerations have been made:

(1) Klur [12] pointed out the appearance of a Q^1 peak located at −76 ppm and assigned as Q^{1p} (Si–O–Ca–O–H groups, see Fig. 6c) but Q^{1p} tetrahedra are only noticed if the CaO/SiO_2 ratio is much greater than 1.0. However, the CaO/SiO_2 ratio of S1 or S2 is lower than 1.0, therefore, it is not expected that the new signal, Q^{2p}(Mg), could be attributed to a Q^{1p} tetrahedra.

(2) The Ca^{2+} ions of interlayer space (Ca labile) might be substituted by the Mg^{2+} ions. Klur [12] described C–S–H gels of similar CaO/SiO_2 ratio, with the interlayer space of the dreierketten pattern, containing Ca^{2+} and H^+, and bonded to the two terminal oxygen of the Q^{2p} tetrahedral. In order to identify the new peak, the correlation of Janes and Oldfield [44] has been applied. This correlation is given by the relationship:

$$\delta^{29}\mathrm{Si} = -24.336\Sigma\mathrm{EN} + 279.27, \quad (1)$$

where EN is the electronegativity: for O–Si = 3.9722, O–Ca = 3.6058, O–Mg = 3.5048, O–H = 3.5882, and the mean absolute deviation between theory and experiment is 1.96 ppm [44].

In this way, the application of Eq. (1) on the two models, with and without Mg in C–S–H, gives: δQ^{2p}(Ca)−

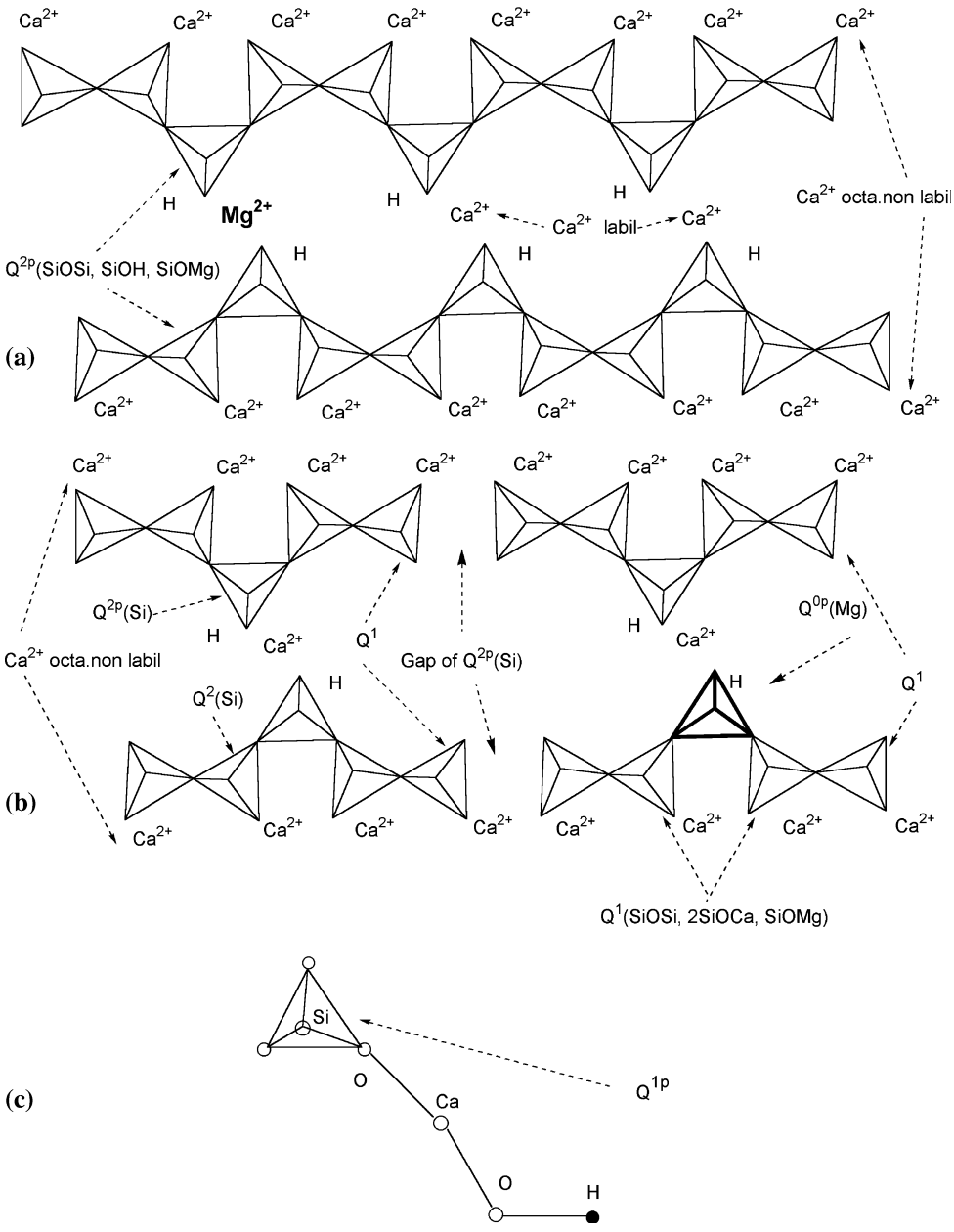

Fig. 6 Localization of the magnesium ions into the "dreierketten" pattern of the CSH gel: for a CaO/SiO_2 ratio < 1.1 (**a**) and a CaO/SiO_2 ratio > 1.1 (**b**). Scheme of Q^{1p} tetrahedra, with two oxygen are linked to a non-labile calcium plane and the –Ca–O–H groups are localized in the interlayer space (**c**) [12]

$\delta Q^{2p}(Mg) = Q^{2p}(SiOSi, SiOH, SiOCa) - Q^{2p}(SiOSi, SiOH, SiOMg) = -2.46$ ppm. This value is close to the chemical shift difference reported in Table 4 for S2, ($\delta Q^{2p}(Ca) = -82.7$ ppm, $\delta(Q^{2p}(Mg)) = -77.5$ ppm) − 5.2 ppm. Consequently, the extra peaks $Q^{2p}(Mg)$ at −77.5 ppm (S2) and −79.1 ppm (S1) might be attributed to a Q^{2p}(SiOSi, SiOH, SiOMg) tetrahedron, which is bonded to magnesium. The resonance of the extra peak [Q^{2p}(SiOSi, SiOH, SiOMg)] is relatively close to the chemical shifts of the Q^2 tetrahedra of enstatite [21]. The structure of enstatite contains single chain silicates with magnesium ions in octahedral sites.

The NMR results for CaO/SiO_2 ratios < 1 show that some magnesium ions would substitute calcium ions in octahedral sites of a C–S–H structure as it is plotted in Fig. 6a. The presence of magnesium into the samples has also been confirmed by SEM–EDAX studies [16].

Structure of C–S–H in the presence of MgO for CaO/SiO_2 ratios > 1

The NMR signal corresponding to the defects (Q^3 defect) which are observed for the lower CaO/SiO_2 ratios, disappear in sample S3, and it is in agreement with the NMR results of Klur [12]. The intensity of the NMR signal from Q^1 tetrahedra increases, and it is attributed to the rupture in the silicate chains [14, 15]. In this way, a gap the Q^{2p} tetrahedra appears.

For sample S3, a new resonance at −78.8 ppm is detected. The new resonance is assigned to a Q^{2p}(SiOSi, SiOH, SiOMg) tetrahedron bonded to a magnesium, similar to those of S1 and S2. The chemical shift of the Q^{2p}(SiOSi, SiOH, SiOMg) is different from 1.3 ppm in respect to the resonance observed in sample S2. This fact might be due to structural changes of C–S–H that appear around $CaO/SiO_2 \cong 1.16$, which would be the frontier between C–S–H (α) and C–S–H (β) [12].

Sample S4 with the highest CaO/SiO_2 ratio shows the NMR signal of a Q^2 tetrahedra, and a well-defined Q^1 peak. The resonance of the Q^{2p} tetrahedra disappears in accordance with [12]. A new resonance (Q^2(Mg)) has also been identified in this sample. This new resonance is observed in the region of the nesosilicates (Q^0) and coexists with the resonance peak of the unreacted anhydrous part of C_3S. The new resonance in S4 (Fig. 4) does not seem to correspond to a crystalline phase. The linewidth at half-height of this one is slightly larger with respect to the Q^0 signal from the anhydrous crystalline C_3S.

A chemical balance for the calcium content has been calculated using the results of the chemical analyses, thermogravimetric data, and the deconvolution of NMR spectrum by supposing that the new signal is C_3S. The results of the chemical balance on the calcium content seems to discard the attribution of this peak to a C_3S residue. In the same way, a new chemical balance on the calcium content has been achieved, but supposing that the new signal might be C_2S, the chemical balance discard this possibility too. Moreover, Gaussian lines of unreacted anhydrous C_3S and the new one have identical intensity, the attribution of this one to C_2S is not supported by XRD diffractogram where C_2S remains as impurities.

Other neglected hypotheses for the new resonance of Q^2(Mg) have been evaluated such as follows:

- Magnesium silicates in the range of the nesosilicates (Q^0), as olivine, chondrodite, and fosterite, are discarded because of their isotropic chemical shifts that are about −60 to −62 ppm [21], which are largely shifted from the new resonance Q^2(Mg) of S4. Moreover, crystalline magnesium silicates are not identified by the XRD here.
- The possibility of a Q^{2p} (SiOSi, SiOH, SiOMg) is discarded, because the new resonance is largely shifted in comparison with the resonance of the Q^{2p} tetrahedron and, in agreement with Klur [12] the deconvolution of the sample S4 ($CaO/SiO_2 > 1.6$) does not denote the presence of Q^{2p} tetrahedral.
- The C–S–H gels of $CaO/SiO_2 > 1.0$, display a resonance at (−76 ppm) [12], attributed to a silicon tetrahedral Q^{1p} (Fig. 6c). The new resonance (Q^2(Mg)) is shifted to 3 ppm from this one, therefore the silicon tetrahedral Q^{1p}(CaOH) is not considered.
- In the same way, the substitution of calcium by magnesium (Q^{1p}(MgOH)) is discarded because following the correlation of Janes and Oldfied [44] the resonance of a Q^{1p}(OCa, OCa, OH, OMg) tetrahedral will give a peak at −68.8 ppm.

Finally the possibility of the incorporation of magnesium ions into the gap of the silicon tetrahedron Q^{2p} (Fig. 6b) has been considered. This fact involves the incorporation of magnesium ions in tetrahedral sites.

To confirm this fact, the correlation of Janes and Oldfield [44] has been applied to the model that is shown in Fig. 6b: $\delta Q^2(Ca) - \delta Q^1(Mg^{IV}) = Q^2(2SiOSi, 2SiOCa) - Q^1$ (SiOSi, 2SiOCa, SiOMg) = +11.38 ppm. The chemical shift difference is close to the experimental value, +12.8 ppm. The incorporation of magnesium ions in tetrahedral position should be equilibrated by calcium atoms because the Loweinstein's rules exclude the balance by magnesium (Mg–O–Mg) (see Fig. 6b). In literature, there are few examples that are related to tetrahedral magnesium sites: $MgAl_2O_4$ [45], $MgSiN_2$ [46], $MgAlSiN_3$ [46], and akermanite [47].

The NMR chemical shifts depend primarily on the atomic nearest neighbor (NN) and next-nearest neighbor (NNN) structures; then, nuclei of atoms in similar local structure resonate at similar chemical shifts. Akermanite

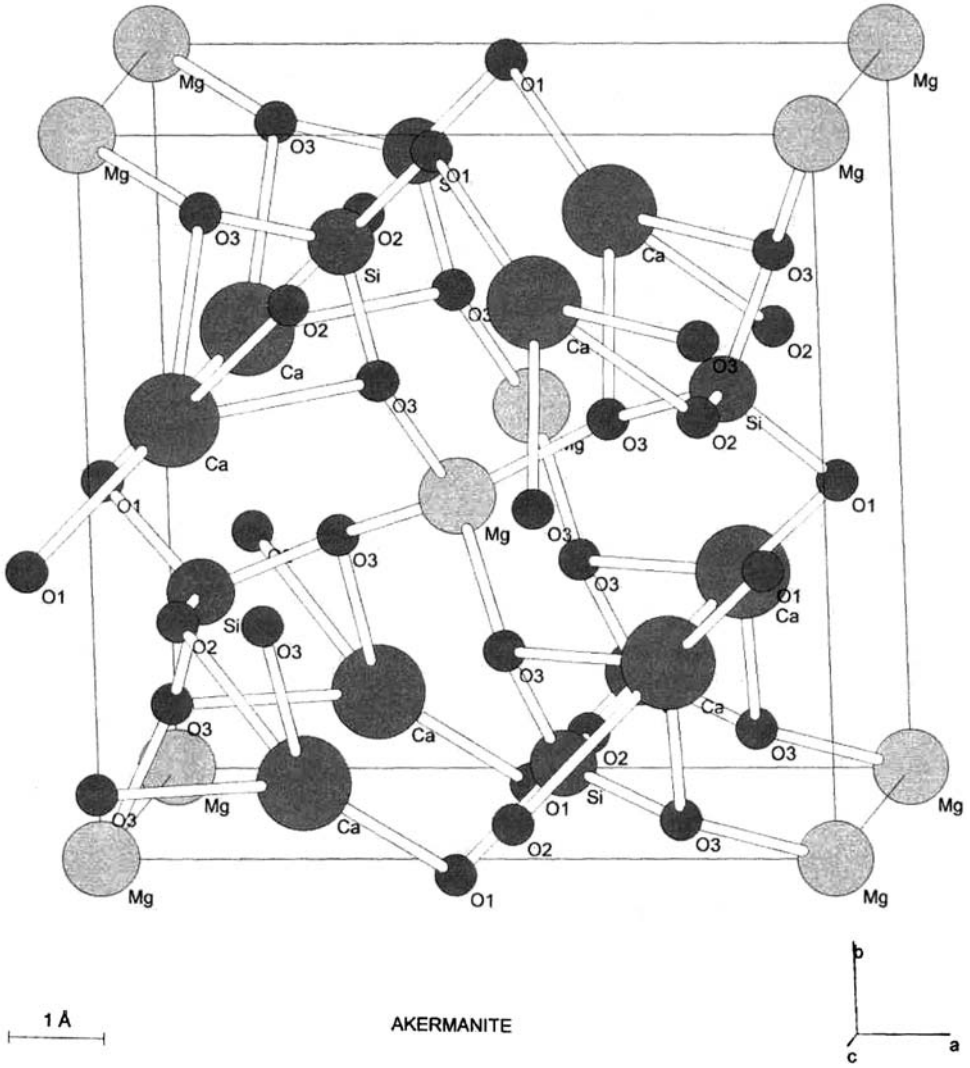

Fig. 7 Structure of akermanite [36]. Spatial group: P421 m. Lattice parameters: a = 7.8338 Å, b = 5.0082 Å, alpha = 90.00°, beta = 90.00°, gamma = 90.00

structure is shown in Fig. 7, which corresponds to a magnesium silicate, catalogued as sorosilicate Si_2O_7 group. In this structure, silicate tetrahedra are connected to magnesium tetrahedra. The ^{29}Si MAS-NMR of akermanite is characterized by an isotropic chemical shift at −73.7 ppm [21], this one is very close to the Q^1(SiOSi, 2SiOCa, SiOMg) (−73.0 ppm). Looking at Fig. 7, the configuration of the network setting around the two coordination spheres of the tetrahedral magnesium into the akermanite structure [48] is similar with that of the pattern of Fig. 6b and deduced from the NMR fitting. Consequently, in the C–S–H gel with $CaO/SiO_2 > 1.6$, magnesium ions might be incorporated into the gap of the Q^{2p} silicon tetrahedron, but the expected number of magnesium tetrahedra into the C–S–H gel is low, because there are two Q^1(SiOSi, 2SiOCa, SiOMg) per each Q^{0p}(Mg) (see Fig. 6b). The incorporation of Mg into this sample has been confirmed by SEM–EDAX [16]. The attribution of this peak to a silicon bonded to tetrahedral magnesium as described in Fig. 6b might be confirmed by Infrared spectroscopy [16], where the Mg–O vibration of the MgO_4 tetrahedra has been observed. This vibration does not correspond to akermanite because no crystalline magnesium silicates have been identified by XRD.

In the sample S4, there exists the possibility of a co-precipitation of C–S–H gel and an amorphous silicate of calcium and magnesium. The amorphous magnesium silicate would have an akermanite-like structure, in which some magnesium ions are in tetrahedral sites.

Conclusions

The aim of this paper is to support that high-resolution solid-state NMR of ^{29}Si MAS-NMR would be able to identify the presence of magnesium in the C–S–H gel as previously demonstrated by SEM-EDAX studies and infrared spectroscopy [16]. The main conclusions obtained in this study are:

(1) The hydration of tricalcium silicate in hydrothermal conditions at 100 °C in the presence of magnesium oxide leads mainly to the precipitation of C–S–H gel, brucite, and a weak presence of portlandite and carbonates.
(2) The deconvolution of ^{29}Si MAS NMR of low C–S–H gels would confirm the dreierketten structure with some defects (Q^3 defect and Q^{2v}).
(3) From the deconvolution of NMR spectra and based on the "defect tobermorite model", some new resonances appear that are interpreted to correspond to the incorporation of the magnesium ions into the structure of the C–S–H gel. The coordination of magnesium depends on the CaO/SiO_2 ratio.
(4) For C–S–H gels with a CaO/SiO_2 ratio < 1, some magnesium ions might be incorporated into the octahedral sites in the interlayer space of the dreierketten pattern. The isotropic chemical shift of the silicon tetrahedra bonded to an octahedral magnesium would be about -77.5 to -79.1 ppm, and assigned as Q^{2p}(SiOSi, SiOH, SiOMg).
(5) For C–S–H gels with a CaO/SiO_2 ratio > 1, some magnesium ions might be incorporated into the gap of the Q^{2p} silicon tetrahedron as tetrahedral magnesium. The isotropic chemical shift of the silicon tetrahedra Q^1(SiOSi, 2SiOCa, SiOMg) bonded to the tetrahedral magnesium would be about -73.0 ppm.

Acknowledgement The authors thank the "Ministerio de Educación y Ciencia" and the C.I.C.Y.T of Spain for the funds provided, as well as to the DG-XII of the E.U: UNICORN Project (BRPR-CT97-0511). We also thank to Dr. C. Vernet (Lafarge Society) for the synthesis of C_3S and to the Department of NMR. Spectroscopy (C.A.I) from the "Universidad Complutense de Madrid" for the testing facilities.

References

1. Taylor HFW (1990) Cement chemistry. Academic Press, London
2. Masse S (1993) PhD: Synthèse Hydrothermal d'Hydrates de Silicate Tricalcique. Analyse Structurale en Phase Solide. Etude Comparative avec les Ciments Utilisés pour Chemiser les Puits de Pétrole, Université Pierre et Marie Curie Paris
3. Flint EP, Wells LS (1934) J Res Natl Bur Stand 12:751
4. Brunauer S, Kantro D, Copeland L (1958) J Am Chem Soc 80:761. doi:10.1021/ja01537a001
5. Greenberg SA, Chang TN (1965) J Phys Chem 69:182. doi:10.1021/j100885a027
6. Greenberg SA, Chang TN, Anderson E (1965) J Phys Chem 64:1151. doi:10.1021/j100838a012
7. Roller PS, Ewin JG (1940) J Am Chem Soc 62:461. doi:10.1021/ja01860a001
8. Taylor HFW (1950) J Chem Soc 726:3682. doi:10.1039/JR9500003682
9. Nonat A (2004) Cem Concr Res 34:1521. doi:10.1016/j.cemconres.2004.04.035
10. Richardson IG (2004) Cem Concr Res 34:1733. doi:10.1016/j.cemconres.2004.05.034
11. Cong X, Kirkpatrick R (1996) J Adv Cem Base Mater 3:144. doi:10.1016/S1065-7355(96)90046-2
12. Klur I (1996) PhD: Etude par RMN de la Structure des Silicates de Calcium Hydratés, Université Pierre et Marie Curie Paris
13. Klur I, Pollet B, Virlet J, Nonat A (1998). In: Colombet P (ed) Nuclear magnetic resonance spectroscopy of cement-based materials. Springer, Berlin
14. Grutzeck M, Benesi A, Fanning B (1989) J Am Ceram Soc 72:665. doi:10.1111/j.1151-2916.1989.tb06192.x
15. Rodger SA, Groves GW, Clayden NJ, Dobson CM (1988) J Am Ceram Soc 71:91. doi:10.1111/j.1151-2916.1988.tb05823.x
16. Fernandez L, Alonso C, Hidalgo A, Andrade C (2005) Adv Cem Res 17:9. doi:10.1680/adcr.17.1.9.58392
17. Pytel Z, Malolepszy J (1997). In: Justnes H (ed) Proc Int Congr Chem Cem 10th, Amarkai AB, Goeteborg
18. Shrivastava OP, Komarneni S, Breval E (1991) Cem Concr Res 21:83. doi:10.1016/0008-8846(91)90034-F
19. Xu G, Lai Z, Qian G, Yang S, Zhou Q (2000) Guisuanyan Xuebao 28:100
20. Massiot D, Thiele H, Germanus A (1994) Bruker Rep 140:43
21. Engelhardt G, Michel D (1987) High-resolution solid-state NMR of silicates and zeolites. Wiley & Sons, Chichester
22. Mägi M, Lippmaa E, Samoson A, Engelhardt G, Grimmer AR (1984) J Phys Chem 88:1518. doi:10.1021/j150652a015
23. Brough AR, Dobson CM, Richardson IG, Groves GW (1994) J Am Ceram Soc 77:593. doi:10.1111/j.1151-2916.1994.tb07034.x
24. Cong X, Kirkpatrick RJ (1993) Cem Concr Res 23:1065. doi:10.1016/0008-8846(93)90166-7
25. Dobson CM, Goberdhan DGC, Ramsay JDF, Rodger SA (1988) J Mater Sci 23:4108. doi:10.1007/BF01106844
26. Noma H, Adachi Y, Yamada H, Nishino T, Matsuda Y, Yokoyama T (1998). In: Colombet P (ed) Nuclear magnetic resonance spectroscopy of cement-based materials. Springer, Berlin
27. Ramanchandran VS, Feldman RF, Beaudoin JJ (1981) Concrete science. Heyden and Son Ltd., Philadelphia, PA
28. Taylor HFW (1986) J Am Ceram Soc 69:464. doi:10.1111/j.1151-2916.1986.tb07446.x
29. Stein HN, Stevels JM (1964) J Appl Chem 14:338
30. Grutzeck MW, Kwan S, Thompson JL, Benesi A (1999) J Mater Sci Lett 18:217. doi:10.1023/A:1006624215448
31. Barnes JR, Clague ADH, Clayden NJ, Dobson CM, Hayes CJ, Groves GW et al (1985) J Mater Sci Lett 4:1293. doi:10.1007/BF00723485
32. Brunet F, Bertani P, Charpentier T, Virlet J, Nonat A (2004) J Phys Chem B 108:15494. doi:10.1021/jp031174g
33. Klur I, Jacquinot JF, Brunet F, Charpentier T, Virlet J, Schneider C et al (2000) J Phys Chem B 104:10162. doi:10.1021/jp001342u
34. Faucon P, Delaye JM, Virlet J (1996) J Solid State Chem 127:92. doi:10.1006/jssc.1996.0361
35. Faucon P, Jacquinot JF, Delaye JM, Virlet J (1997) Philos Mag B 75:769. doi:10.1080/13642819708202353
36. Skibsted J, Jakobsen HJ, Hall C (1995) J Chem Soc-Faraday Trans 91:4423. doi:10.1039/ft9959104423
37. Edwards CL, Alemany LB, Barron AR (2007) Ind Eng Chem Res 46:5122. doi:10.1021/ie070220m
38. Stephan D, Wistuba S (2006) J Eur Ceram Soc 26:141. doi:10.1016/j.jeurceramsoc.2004.10.031
39. Peterson VK, Hunter BA, Ray A (2004) J Am Ceram Soc 87:1625
40. De La Torre AG, Bruque S, Campo J, Aranda MAG (2002) Cem Concr Res 32:1347. doi:10.1016/S0008-8846(02)00796-2
41. De La Torre AG, Bruque S, Aranda MAG (2001) J Appl Crystallogr 34:196. doi:10.1107/S0021889801002485
42. Mumme WG (1995) Neues Jahrb Mineral-Montash Hefte 4:145

43. Clayden NJ, Dobson CM, Groves GW, Rodger SA (1986). In: Secr (ed) Congr Int Quim Cimento 8th, Geral 8o CIQC, Rio de Janeiro
44. Janes N, Oldfield E (1985) J Am Chem Soc 107:6769. doi:10.1021/ja00310a004
45. Dupree R, Smith ME (1988) J Chem Soc Chem Commun 22:1483. doi:10.1039/C39880001483
46. MacKenzie KJD, Meinhold RH (1994) J Mater Chem 4:1595. doi:10.1039/jm9940401595
47. Fiske PS, Stebbins JF (1994) Am Mineral 79:848
48. Yang H, Hazen RM, Downs RT, Finger LW (1997) Phys Chem Miner 24:510. doi:10.1007/s002690050066